Linear and second order optics corrections for the KEK Accelerator Test Facility final focus beam line

T. Okugi,[1] S. Araki,[1] P. Bambade,[2] K. Kubo,[1] S. Kurado,[1] M. Masuzawa,[1] E. Marin,[3] T. Naito,[1] T. Tauchi,[1] N. Terunuma,[1] R. Tomas,[4] J. Urakawa,[1] G. White,[3] and M. Woodley[3]

[1]*High Energy Accelerator Research Organization (KEK), Tsukuba, Ibaraki 305-0801, Japan*
[2]*LAL, Universite Paris-Sud, CNRS/IN2P3, Orsay, France*
[3]*SLAC National Accelerator Laboratory, Menlo Park, California 94025, USA*
[4]*European Organization for Nuclear Research (CERN), Geneva, Switzerland*

(Received 2 October 2013; published 24 February 2014)

In this paper, the linear and second order optics corrections for the KEK Accelerator Test Facility (ATF2) final focus beam line are described. The beam optics of the ATF2 beam line is designed based on a local chromaticity correction scheme similar to the ILC final focus system. Beam measurements in 2012 revealed skew sextupole field errors that were much larger than expected from magnetic field measurements. The skew sextupole field error was a critical limitation of the beam size at the ATF2 virtual interaction point (IP). Therefore, four skew sextupole magnets were installed to correct the field error in August 2012. By using the four skew sextupole magnets, the predicted tolerances of the skew sextupole field errors of the ATF2 magnets were increased. Furthermore, analyzing field maps of the sextupole magnets identified the source of the skew sextupole field error. After the field error source was removed, the IP vertical beam size could more easily be focused to less than 65 nm.

DOI: 10.1103/PhysRevSTAB.17.023501 PACS numbers: 29.20.Ej, 29.27.−a, 42.15.Fr, 41.85.−p

I. INTRODUCTION

The KEK Accelerator Test Facility (KEK-ATF) [1,2] has been built for accelerator research and development, especially for the International Linear Collider (ILC) [3]. Figure 1 shows a schematic view of the KEK-ATF accelerator complex. KEK-ATF consists of an injector linac, a damping ring, a beam extraction line, and ATF2 beam line. The purpose of the damping ring is to supply a low emittance beam to the extraction line and ATF2 beam line for accelerator research and development. The vertical beam emittance produced by the damping ring is less than 10 pm [4,5] (smaller than the 12 pm ATF2 requirement). The corresponding 30 nm normalized emittance is comparable to the requirement of the ILC beam delivery system. The ATF2 beam line was constructed to study the ILC final focus system, utilizing the small emittance beam generated by the damping ring.

II. ATF2 BEAM LINE

A. Beam optics of the ATF2 beam line

The ILC final focus system is designed based on the local chromaticity correction technique [6]. The main purpose of the ATF2 beam line is to demonstrate beam focusing with the local chromaticity correction method, and to establish a beam tuning method for linear collider final focus systems. Therefore, the ATF2 beam optics was designed based on the local chromaticity correction scheme of the ILC final focus system. The beam optics for the ILC and ATF2 beam lines are shown in Fig. 2 (the main parameters are listed in Table I). The chromaticity of the ATF2 beam line is designed to be comparable to the ILC final focus system with a resulting design IP vertical beam size of 37 nm. The ATF2 beam line was operated with a 10 times larger horizontal IP beta-function (β_x^*) optics than originally designed to reduce the effect of multipole field errors to be comparable to the tolerances of the ILC final focus design. This optics is

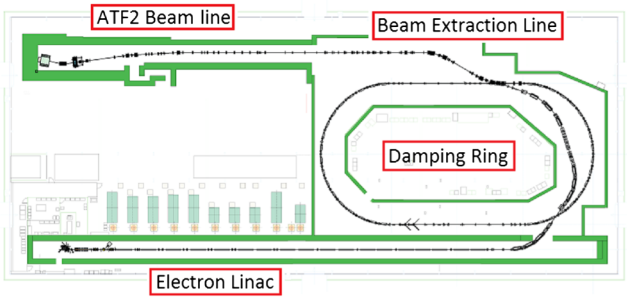

FIG. 1. Accelerator complex of KEK-ATF, consisting of an electron linac, a damping ring, a beam extraction line, and the ATF2 beam line.

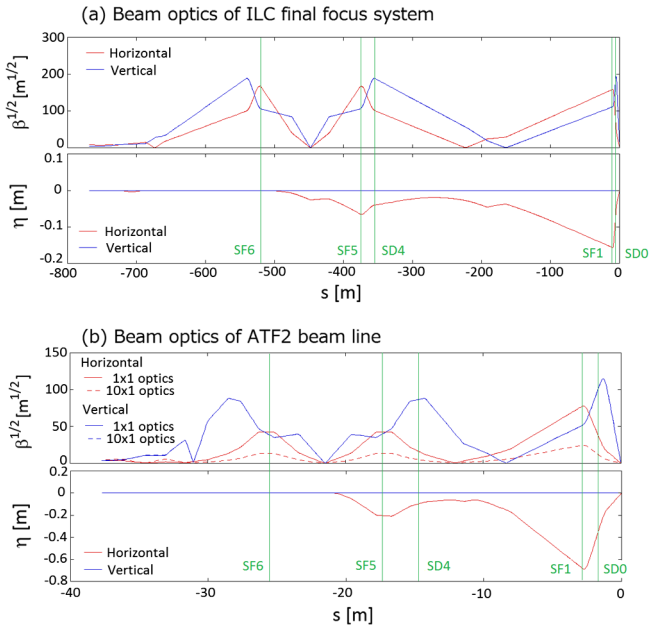

FIG. 2. Beam optics of the ILC final focus beam line (a) and the ATF2 beam line (b). Both the 1×1 optics and the 10×1 optics are shown.

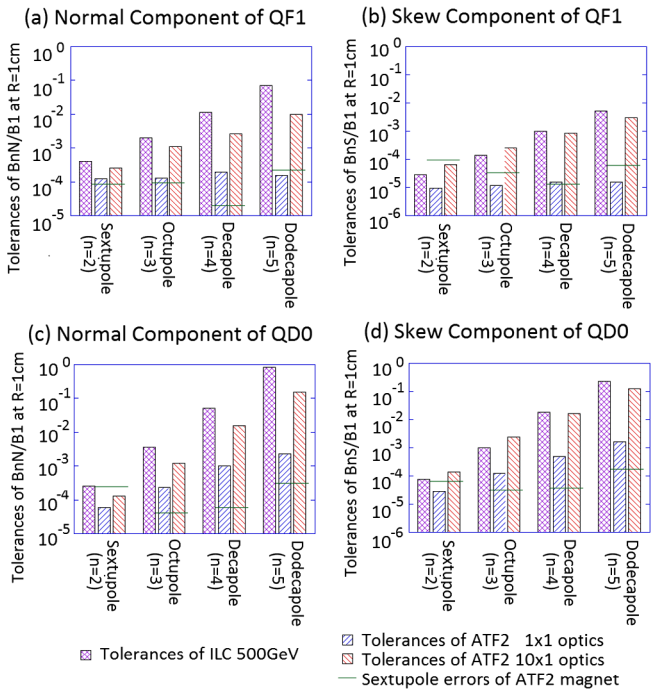

FIG. 3. Tolerances of multipole field errors for the final doublet (QF1 and QD0) of the ILC and ATF2 final focus beam lines. The tolerances are defined as the error of each component required to induce a 2% IP vertical beam size growth. The multipole field errors in the ATF2 magnets are also plotted. Since the bore radius of the ATF2 final doublet magnets are much larger than ILC, the multipole fields of the ATF2 final doublet are measured at R = 2 cm and scaled to R = 1 cm.

referred to as the "10×1 optics" because of the 10 times larger β_x^* and the same β_y^* compared with the original design, while the original optics is labeled "1×1 optics." Final doublet (QF1, QD0) multipole field error tolerances for ILC and ATF2 are shown in Fig. 3. Sextupole field error tolerances for all quadrupole magnets, for ILC and ATF2, are shown in Fig. 4. The tolerances are defined as the error required to induce a 2% IP vertical beam size growth. The multipole field errors measured in the ATF2 magnets are also plotted in Figs. 3 and 4. The tolerances of the magnets in the 10×1 optics are comparable to those of ILC and for most of the quadrupole magnets are larger than the measured multipole field errors.

B. IP beam size monitor for ATF2

A nanometer scale beam size monitor (proposed in [7]) was demonstrated at SLAC Final Focus Test Beam (FFTB) during the 1990s [8], measuring a beam size of approximately 70 nm. This IP beam size monitor (IP-BSM) used at FFTB was modified and installed at the ATF2 IP. The IP-BSM uses a fringe pattern formed by two interfering laser beams. The laser fringe pitch is defined by the wavelength (λ) and crossing angle of the two laser paths (θ): $d = \lambda/2\sin(\theta/2)$. Compton scattered photons from the transverse overlap of the laser fringe pattern with the beam are measured downstream of the IP. The signal modulation depth is written as a function of the IP vertical beam size (σ_y):

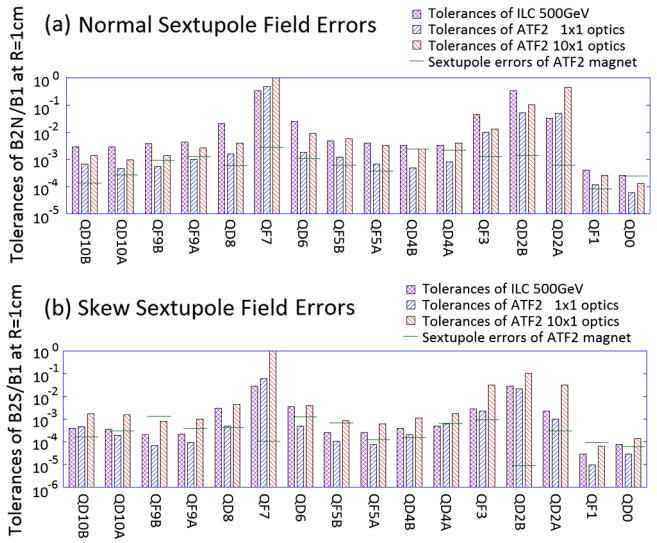

FIG. 4. Tolerances of sextupole field errors for all quadrupole magnets in the ILC and ATF2 final focus beam lines. The tolerances are defined as the error of each magnet required to induce a 2% IP vertical beam size growth. The measured multipole field errors of the ATF2 magnets are also plotted.

TABLE I. Beam and optics parameters for the ILC and ATF2 final focus beam lines.

		ATF2	
	ILC 500 GeV	Original (1×1 optics)	Present (10×1 optics)
E[GeV]	250	1.28	
ε_x[nm]/ε_y[pm]	0.02/0.07	2/12	
$\gamma\varepsilon_x$[μm]/$\gamma\varepsilon_y$[μm]	10/0.035	5/0.030	
σ_p/p	0.12%	0.08%	
L*[m]	3.5	1	
β_x[mm]/β_y[mm]	11/0.48	4/0.1	40/0.1
σ_x[μm]/σ_y[nm]	0.47/5.9	2.8/37	8.9/37
$\xi_y \sim$ L$^*/\beta_y$	7,300	10,000	
$\xi_y \times \sigma_p/p$	8.75	8.00	

$$M = C|\cos\theta|\exp[-2(k_y\sigma_y)^2], \quad k_y = \frac{\pi}{d}, \tag{1}$$

where C expresses the contrast reduction of the laser fringe pattern. Reduction of the laser fringe contrast is caused by deteriorated laser spatial coherency, mismatch in the overlap of the two laser beams, etc. Since the modulation depth of the Compton signal is also reduced by$C$, this is referred to as the modulation reduction factor. From Eq. (1), the beam size is expressed as a function of the modulation depth:

$$\sigma_y = \frac{1}{k_y}\sqrt{\frac{1}{2}\ln\left(\frac{C|\cos\theta|}{M}\right)}. \tag{2}$$

We can measure the modulation depth of the Compton signal by measuring its strength for various relative beam positions with respect to the laser fringe. Then, we can evaluate the IP beam size from the measured modulation depth using Eq. (2). For ATF2, the laser wavelength used in the IP-BSM was changed from 1064 nm to 532 nm to reduce the laser fringe pitch, and three laser crossing modes (2–8° degree mode, 30° mode, 174° mode) were prepared to increase the range of possible beam size measurements [9]. The dynamic ranges of the IP-BSM at ATF2 are shown in Fig. 5.

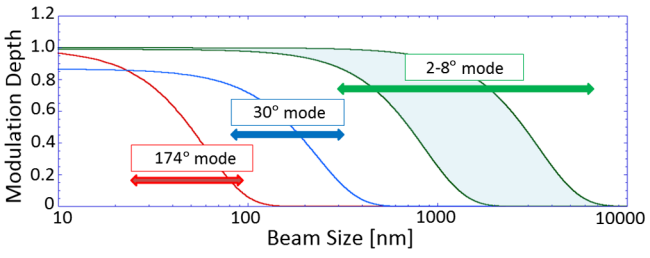

FIG. 5. Dynamic ranges of the IP-BSM at the ATF2 IP. 3 laser crossing modes are plotted.

III. ATF2 BEAM SIZE TUNING STATUS IN JUNE 2012

A. Liner optics tuning knobs

There are five sextupole magnets (SF6, SF5, SD4, SF1, and SD0) in the ATF2 beam line, as in the ILC final focus beam line (see Fig. 2). The transverse positions of all the sextupole magnets are controlled using magnet movers. When a sextupole magnet is moved horizontally, a quadrupole field is generated. The strength of the generated quadrupole field is proportional to the horizontal offset and changes the horizontal and vertical beam waists (W_x and W_y), IP horizontal dispersion η_x, and its derivative η'_x. The linear optics tuning knobs of P_{AX} (W_x knob), P_{AY} (W_y knob), P_{EX} (η_x knob), and P_{EPX} (η'_x knob) are calculated as orthogonal sets of horizontal offsets of the sextupole magnets, only individually changing W_x, W_y, η_x, and η'_x, respectively [10].

When a sextupole magnet is moved vertically, a skew quadrupole field is generated. The strength of the generated skew quadrupole field is proportional to the vertical offset and changes the vertical dispersion η_y, the derivative η'_y, and xy coupling components at the IP, especially $\langle x'y\rangle$. The linear optics tuning knobs of P_{EY} (η_y knob), P_{EPY} (η'_y knob), and P_{32} ($\langle x'y\rangle$ knob) are calculated as orthogonal sets of the vertical offsets of the sextupole magnets, only individually changing η_y, η'_y, and $\langle x'y\rangle$, respectively.

The IP vertical beam size is sensitive to the beam waist position offset (W_y), the IP vertical dispersion (η_y), and the amount of xy coupling at the IP ($\langle x'y\rangle$) and are used for IP vertical beam size tuning during ATF2 beam operations. The IP vertical beam size can be expressed as

$$\sigma_y^2 = \varepsilon_y\beta_y^* + (\sigma_{AY} + P_{AY})^2 + (\sigma_{EY} + P_{EY})^2 + (\sigma_{32} + P_{32})^2 + \Delta\sigma_{y,MP}^2,$$

$$\sigma_{AY} = \sqrt{\frac{\varepsilon_y}{\beta_y^*}}W_y, \quad \sigma_{EY} = \delta\eta_y, \quad \sigma_{32} = \sqrt{\frac{\beta_x^*}{\varepsilon_x}}\langle x'y\rangle, \tag{3}$$

where P_{AY}, P_{EY}, and P_{32} are amplitudes of the beam waist knob, the vertical dispersion knob, and the xy coupling

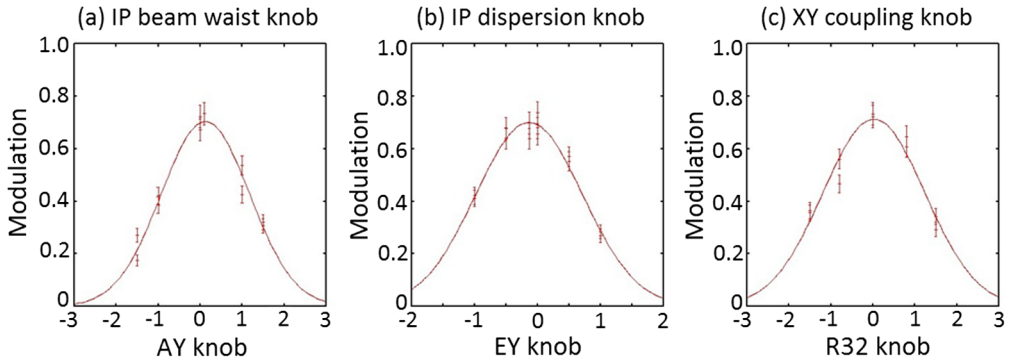

FIG. 6. Example of IP beam size tuning using linear knobs. The beam size tuning was done with IP-BSM 2-8° mode.

knobs $\langle x'y\rangle$, respectively. $\Delta\sigma_{y,MP}$ is the IP beam size contribution due to multipole field errors. Inserting Eq. (3) into Eq. (1), the modulation depth can be expanded as

$$\begin{aligned} M = C|\cos\theta| \exp[-2k_y^2(\varepsilon_y\beta_y^* + \Delta\sigma_{y,MP}^2)] \\ \times \exp\left[-2k_y^2(\sigma_{AY} + P_{AY})^2\right] \\ \times \exp\left[-2k_y^2(\sigma_{EY} + P_{EY})^2\right] \\ \times \exp[-2k_y^2(\sigma_{32} + P_{32})^2]. \end{aligned} \quad (4)$$

The first line of Eq. (4) is the maximum amplitude of the modulation depth, corresponding to the minimum achievable beam size after application of the linear knob corrections. The second to fourth lines of Eq. (4) are the responses of the linear knobs. Examples of IP beam size tuning with the linear knobs are shown in Fig. 6. The modulation depth exhibits a Gaussian response to the linear knobs, as can be seen from Eq. (4). The optimum setting of a linear knob corresponds to the peak of the fitted Gaussian function.

A particle tracking simulation was written to evaluate ATF2 tuning performance using the linear knobs using the simulation software SAD [11]. Errors were introduced to reproduce the present performance of the ATF2 beam line. Multipole field errors from magnetic field measurements of all quadrupoles, sextupoles, and bending magnets in the ATF2 beam line were incorporated. Misalignment and field strength errors, accuracies of beam position monitor offset adjustments with respect to adjacent magnetic centers [beam based alignment (BBA)], and IP-BSM accuracies assumed in the simulation are listed in Table II. Since a wire scanner monitor is also used for measuring the beam size at the IP, the accuracy of this is also listed in the table. The simulation was performed using 100 random seeds. The procedure of the IP beam size tuning in the simulation is the same as the actual ATF2 tuning procedure. The strength of QF1 is adjusted to make $\eta_x^* \approx 0$, and the IP horizontal beam waist is optimized using theW_x knob. The initial vertical waist was adjusted by changing the strength of QD0, and the initial xy coupling ($\langle x'y\rangle$) was adjusted by rolling QD0 and measuring the vertical beam size at the IP using the wire scanner. The linear knob tuning procedure using the IP-BSM is then carried out. This was iterated for the three different IP-BSM laser crossing modes.

TABLE II. Error distributions for the beam tuning simulation.

Quadrupole Sextupole	Misalignment	Δx	100 μm (Gaussian)
		Δy	100 μm (Gaussian)
		$\Delta\theta$	200 μrad (Gaussian)
	Strength Error	ΔK	0.1% (Gaussian)
Bend	Misalignment	$\Delta\theta$	200 μrad (Gaussian)
	Strength Error	ΔK	0.1% (Gaussian)
BBA Accuracy			$\pm$100 μm (uniform)
IP-BSM Accuracies	2–8 degree mode		$\pm$100 nm (uniform)
	30 degree mode		$\pm$20 nm (uniform)
	174 degree mode		$\pm$8 nm (uniform)
Wire Scanner Accuracy			$\pm$ 800 nm (uniform)

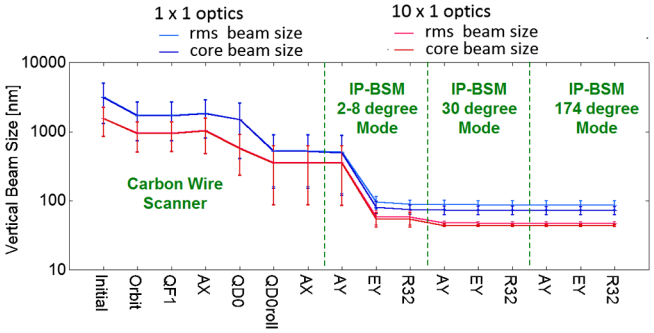

FIG. 7. Simulation results showing beam size changes throughout the beam tuning procedure for the 1×1 optics and 10×1 optics. "rms beam size" is the standard deviation of the y distribution of the tracked particles at the IP. "Core beam size" is the width of a Gaussian function fitted to the core of this distribution.

The simulation results of the vertical beam size changes throughout the beam tuning procedure for both the 1×1 optics and the 10×1 optics are shown in Fig. 7. The final beam sizes after the linear knob tuning are listed in Table III. The vertical beam size at the IP is tuned below 50 nm for the 10×1 optics using only the linear knobs, but does not converge to this level with the 1×1 optics using the linear knobs alone.

B. Effect of skew sextupole field errors

The beam tuning simulation for the 10×1 optics shows the feasibility of achieving a vertical beam size at the IP of below 50 nm using linear knobs alone; however, the IP beam size could not be focused below 150 nm experimentally using only the linear knobs. Therefore, we installed a skew sextupole magnet (SK3 in Fig. 8) in order to increase the tolerances of skew sextupole field errors in January 2011 [12]. We tried to reduce the IP beam size further by using SK3 several times during beam operations in 2012. The results are shown in Fig. 9. The magnet strength to maximize the IP-BSM modulation was around $K_{2S} = 0.5$ m^{-2}. It was suggested

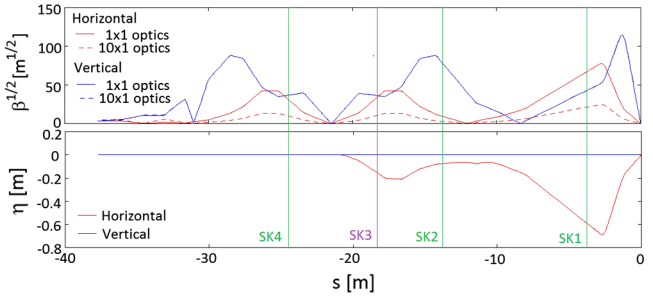

FIG. 8. Location of skew sextupole magnets (SK1-SK4). SK3 was installed in January 2011; the other SKs were installed in August 2012.

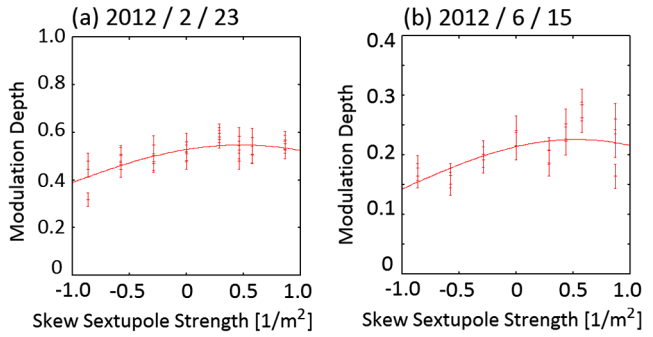

FIG. 9. The observed IP-BSM modulation dependence on the strength of the skew sextupole magnet SK3.

that there were strong skew sextupole field errors present somewhere in the beam line.

IV. BEAM SIZE TUNING WITH SECOND ORDER OPTICS KNOBS

A. Second order optics tuning knobs

The strengths of the sextupole magnets in the final focus beam line are set for cancelling chromatic and geometrical aberrations [6]. Other second order aberrations can also be generated, for example, if there are sextupole field errors present in any magnets. When there is a sextupole field

TABLE III. Simulated beam size with only linear knobs for the original ATF2 optics and the present ATF2 optics. "rms beam size" is the standard deviation of the y distribution of the tracked particles at the IP. "Core beam size" is the width of a Gaussian function fitted to the core of this distribution. The $\pm$ shows the standard deviation of the simulated beam size at the IP.

			$\sigma_x^*[\mu\text{m}]$	$\sigma_y^*[\mu\text{m}]$
Original (1×1 optics)	Linear calculation		2.83	34.6
	Simulation	rms	4.17 ± 0.32	86.9 ± 13.2
		core	3.50 ± 0.26	72.2 ± 10.1
Present (10×1 optics)	Linear calculation		8.94	34.6
	Simulation	rms	9.24 ± 0.07	47.1 ± 2.5
		core	9.16 ± 0.07	43.5 ± 1.6

error (ΔK_{SN}), the IP horizontal and vertical positions are changed as a function of the particle positions at the sextupole magnet x, y and the momentum offset δ:

$$\Delta x_{IP} = \frac{R_{12}\Delta K_{2N}}{2}(x^2 + 2\eta_x x\delta + \eta_x^2\delta^2 - y^2), \quad (5)$$

$$\Delta y_{IP} = R_{34}\Delta K_{2N}(xy + \eta_x y\delta). \quad (6)$$

Furthermore, when the sextupole error sources are located at the large beta function region from where the betatron phase advances to the IP are almost $(n + 1/2)\pi$ (n; integer), the horizontal and vertical positions at the error sources are strongly correlated to the horizontal and vertical angles at the IP, x'_{IP} and y'_{IP}:

$$x = -R_{12}x'_{IP}, \quad (7)$$

$$y = -R_{34}y'_{IP}, \quad (8)$$

where R_{12} and R_{34} are 1-2 and 3-4 components of the transfer matrix from the location of the field error to the IP. Therefore, the horizontal and vertical position change at the IP by the sextupole field errors can be expressed as

$$\Delta x_{IP} = P_{X22}x'^2_{IP} + P_{X26}x'_{IP}\delta + P_{X66}\delta^2 + P_{X44}y'^2_{IP}, \quad (9)$$

$$\begin{aligned}
&\Delta y_{IP} = P_{Y24}x_{IP}y_{IP} + P_{Y46}y_{IP}\delta,\\
&P_{X22} = \sum\frac{\Delta K_{2N}R_{12}^3}{2}, \qquad P_{X26} = -\sum\Delta K_{2N}R_{12}^2\eta_x,\\
&P_{X66} = \sum\frac{\Delta K_{2N}R_{12}\eta_x^2}{2}, \qquad P_{X44} = -\sum\frac{\Delta K_{2N}R_{12}R_{34}^2}{2},\\
&P_{Y24} = \sum\Delta K_{2N}R_{12}R_{34}^2, \qquad P_{Y46} = -\sum\Delta K_{2N}R_{34}^2\eta_x,
\end{aligned} \quad (10)$$

Furthermore, the square of the beam sizes can be expressed from Eqs. (9), (10):

$$\begin{aligned}
\Delta\sigma^{*2}_{x,SN} &= \langle\Delta x^2_{IP,SN}\rangle\\
&= 3P^2_{X22}\sigma^{*4}_{x'} + 3P^2_{X44}\sigma^{*4}_{y'} + 3P^2_{X66}\sigma^4_\delta\\
&\quad + (P^2_{X26} + 2P_{X22}P_{X66})\sigma^{*2}_{x'}\sigma^2_\delta\\
&\quad + 2P_{X22}P_{X44}\sigma^{*2}_{x'}\sigma^{*2}_{y'} + 2P_{X44}P_{X66}\sigma^{*2}_{y'}\sigma^2_\delta
\end{aligned} \quad (11)$$

$$\Delta\sigma^{*2}_{y,SN} = \langle\Delta y^2_{IP,SN}\rangle = P^2_{Y24}\sigma^{*2}_{x'}\sigma^{*2}_{y'} + P^2_{Y46}\sigma^{*2}_{y'}\sigma^2_\delta, \quad (12)$$

where $\sigma^*_{x'}$, $\sigma^*_{y'}$ are the beam divergences at the IP and σ_δ is the energy spread. Change of the second order beam parameters at the IP can be expressed as

$$x_{22} \equiv \frac{\langle\Delta x_{IP,SN}x'^2_{IP}\rangle}{\sigma^{*2}_{x'}} = 3P_{X22}\sigma^{*2}_{x'} + P_{X44}\sigma^{*2}_{y'} + P_{X44}\sigma^{*2}_{y'} \quad (13)$$

$$y_{24} \equiv \frac{\langle\Delta y_{IP,SN}x'_{IP}y'_{IP}\rangle}{\sigma^*_{x'}\sigma^*_{y'}} = P_{Y24}\sigma^*_{x'}\sigma^*_{y'}, \quad (14)$$

and so on. Therefore, we can express the relationships between the sextupole field error and the second order beam parameters at the IP as

$$\begin{pmatrix} x_{22}\\ x_{26}\\ x_{44}\\ x_{66}\end{pmatrix} = \begin{pmatrix} 3 & 0 & 1 & 1\\ 0 & 1 & 0 & 0\\ 1 & 0 & 3 & 1\\ 1 & 0 & 1 & 3\end{pmatrix}\begin{pmatrix} P_{X22}\sigma^{*2}_{x'}\\ P_{X26}\sigma^*_{x'}\sigma_\delta\\ P_{X44}\sigma^{*2}_{y'}\\ P_{X66}\sigma^2_\delta\end{pmatrix}, \quad (15)$$

$$\begin{pmatrix} P_{X22}\sigma^{*2}_{x'}\\ P_{X26}\sigma^*_{x'}\sigma_\delta\\ P_{X44}\sigma^{*2}_{y'}\\ P_{X66}\sigma^2_\delta\end{pmatrix} = \frac{1}{10}\begin{pmatrix} 4 & 0 & -1 & -1\\ 0 & 1 & 0 & 0\\ -1 & 0 & 4 & -1\\ -1 & 0 & -1 & 4\end{pmatrix}\begin{pmatrix} x_{22}\\ x_{26}\\ x_{44}\\ x_{66}\end{pmatrix}, \quad (16)$$

and

$$\begin{pmatrix} y_{24}\\ y_{46}\end{pmatrix} = \begin{pmatrix} P_{Y24}\sigma^*_{x'}\sigma^*_{y'}\\ P_{Y46}\sigma^*_{y'}\sigma_\delta\end{pmatrix}. \quad (17)$$

The horizontal and vertical beam size growths at the IP by the sextupole field errors can be expanded by inserting Eqs. (16) and (17) into Eqs. (11) and (12):

$$\begin{aligned}
\Delta\sigma^{*2}_{x,SN} &= \frac{2}{5}(x^2_{22} + x^2_{44} + x^2_{66})\\
&\quad - \frac{1}{5}(x_{22}x_{44} + x_{44}x_{66} + x_{66}x_{22}) + x^2_{26},
\end{aligned} \quad (18)$$

$$\Delta\sigma^{*2}_{y,SN} = y^2_{24} + y^2_{46}. \quad (19)$$

In order to correct the second order optics errors, tuning knobs to correct second order aberrations were prepared. There are five normal sextupole magnets in the ATF2 final focus beam line (see Fig. 2). On the other hand, the number of parameters that affect the horizontal and vertical beam size growth at the IP is six (x_{22}, x_{44}, x_{66}, x_{26}, y_{24}, and y_{46}), from Eqs. (18) and (19). Therefore, x_{44} is ignored to make the ATF2 IP beam size tuning knobs because the effect of x_{44} is expected to be insignificant. Tuning knobs to correct sextupole field error components (X_{22}, X_{26}, X_{66}, Y_{24}, and Y_{46}) are calculated as orthogonal sets of strength changes of 5 sextupole magnets changing only x_{22}, x_{26}, x_{66}, y_{24}, and y_{46}, respectively. Horizontal and vertical beam

size growth at the IP with second order field errors and optics knobs are expressed as

$$\begin{aligned}\Delta\sigma^{*2}_{x,SN} =& \frac{2}{5}[(x_{22}+X_{22})^2+(x_{44}+X_{44})^2+(x_{66}+X_{66})^2] \\ &-\frac{1}{5}[(x_{22}+X_{22})(x_{44}+X_{44})] \\ &-\frac{1}{5}[(x_{44}+X_{44})(x_{66}+X_{66})] \\ &-\frac{1}{5}[(x_{66}+X_{66})(x_{22}+X_{22})]+(x_{26}+X_{26})^2,\end{aligned} \tag{20}$$

$$\Delta\sigma^{*2}_{y,SN} = (y_{24}+Y_{24})^2+(y_{46}+Y_{46})^2, \tag{21}$$

where X_{44} is a linear combination of the second order knobs,

$$X_{44} = a_{22}X_{22}+a_{26}X_{26}+a_{66}X_{66}+b_{24}Y_{24}+b_{46}Y_{46}, \tag{22}$$

where a_{ij} and b_{ij} are the constant coefficients. Furthermore, skew sextupole errors in the beam line induce vertical beam size growth at the IP as well as the normal sextupole field errors. Horizontal beam size change due to the skew sextupole fields is expected to be small and ignored here. Vertical beam size growth at the IP due to the skew sextupole field errors (ΔK_{SK}) can be expressed as

$$\begin{aligned}\Delta\sigma^{*2}_{y,SK} =& \frac{2}{5}(y_{22}^2+y_{44}^2+y_{66}^2) \\ &-\frac{1}{5}(y_{22}y_{44}+y_{44}y_{66}+y_{66}y_{22})+y_{26}^2\end{aligned}$$

$$\begin{pmatrix} y_{22} \\ y_{26} \\ y_{44} \\ y_{66} \end{pmatrix} = \begin{pmatrix} 3 & 0 & 1 & 1 \\ 0 & 1 & 0 & 0 \\ 1 & 0 & 3 & 1 \\ 1 & 0 & 1 & 3 \end{pmatrix} \begin{pmatrix} P_{Y22}\sigma^{*2}_{x'} \\ P_{Y26}\sigma^{*}_{x'}\sigma_{\delta} \\ P_{Y44}\sigma^{*2}_{y'} \\ P_{Y66}\sigma^{2}_{\delta} \end{pmatrix}$$

$$\begin{aligned}P_{Y22} &= \sum\frac{\Delta K_{2S}R_{12}^2R_{34}}{2}, \quad P_{Y26} = -\sum\Delta K_{2S}R_{12}R_{34}\eta_x, \\ P_{Y66} &= \sum\frac{\Delta K_{2S}R_{34}\eta_x^2}{2}, \quad P_{Y44} = -\sum\frac{\Delta K_{2S}R_{34}^3}{2}.\end{aligned} \tag{23}$$

Since we suspected strong skew sextupole field errors in the ATF2 beam line (see Fig. 9), we installed three more skew sextupole magnets in August 2012, making a total of four skew sextupole magnets (SK1-SK4) installed into the beam line. The arrangement of the skew sextupole magnets is shown in Fig. 8. The tuning knobs to correct skew sextupole field error components (Y_{22}, Y_{44} Y_{66}, and Y_{26}) are calculated as orthogonal sets of strength changes of four sextupole magnets changing only y_{22}, y_{44} y_{66}, and y_{26} in Eq. (23), respectively. The vertical beam size growth at the IP from the normal and skew sextupole field errors and second order optics knobs is expressed as

$$\begin{aligned}\Delta\sigma^{*2}_{y} =& \frac{2}{5}[(y_{22}+Y_{22})^2+(y_{44}+Y_{44})^2+(y_{66}+Y_{66})^2] \\ &-\frac{1}{5}[(y_{22}+Y_{22})(y_{44}+Y_{44})]+(y_{24}+Y_{24})^2 \\ &-\frac{1}{5}[(y_{44}+Y_{44})(y_{66}+Y_{66})]+(y_{46}+Y_{46})^2 \\ &-\frac{1}{5}[(y_{66}+Y_{66})(y_{22}+Y_{22})]+(y_{26}+Y_{26})^2.\end{aligned} \tag{24}$$

In order to minimize the IP beam size, the second order knobs should be set to

$$Y_{ij} = -y_{ij} \quad (i,j = 2,4,6). \tag{25}$$

The change of the square of the beam size is proportional to the square of the strength of the knob, and can be expressed as

$$\Delta\sigma^{*2}_{y} = A_{ij}(y_{ij}+Y_{ij}+B_{ij})^2+\sigma^{*2}_{y,ij}, \tag{26}$$

where A_{ij}, B_{ij}, and $\sigma_{y,ij}$ are not changed in the Y_{ij} knob scan. For example, $i = j = 2$,

$$\begin{aligned}\Delta\sigma^{*2}_{y} =& \frac{2}{5}\left[y_{22}+Y_{22}-\frac{(y_{44}+V_{44})+(y_{66}+V_{66})}{3}\right]^2 \\ &+\frac{3}{8}(y_{44}+V_{44})^2+\frac{3}{8}(y_{66}+V_{66})^2+(y_{24}-V_{24})^2 \\ &+(y_{26}-V_{26})^2-\frac{1}{5}[(y_{44}+Y_{44})(y_{66}+Y_{66})] \\ &+(y_{46}+Y_{46})^2.\end{aligned} \tag{27}$$

Therefore, the modulation can be expressed for each knob scan by inserting Eq. (26) into Eq. (1):

$$M \propto \exp[-2k_y^2A_{ij}(y_{ij}+V_{ij}+B_{ij})^2]. \tag{28}$$

The IP-BSM measured modulation depth varies according to a Gaussian function versus the second order optics knob as in the case of the linear knobs. The optimum setting of a second order optics knob corresponds to the peak of the fitted Gaussian function. Because of cross terms, it is not possible to make all knobs completely orthogonal. However, the second order optics knobs can be optimized through iteration.

The orthogonality of the IP beam size tuning knobs was tested by a particle tracking simulation using SAD. In the simulation, the linear optics parameters were evaluated using the particle position and angle distribution at the IP:

$$\alpha_y = -\langle(y-\langle y\rangle)(y'-\langle y'\rangle)\rangle/\varepsilon_y \tag{29}$$

$$\eta_y = \langle(y-\langle y\rangle)(\delta-\langle\delta\rangle)\rangle/\langle(\delta-\langle\delta\rangle)^2\rangle \tag{30}$$

$$R_{32} = \langle(y-\langle y\rangle)(x'-\langle x'\rangle)\rangle/\langle(x'-\langle x'\rangle)^2\rangle, \tag{31}$$

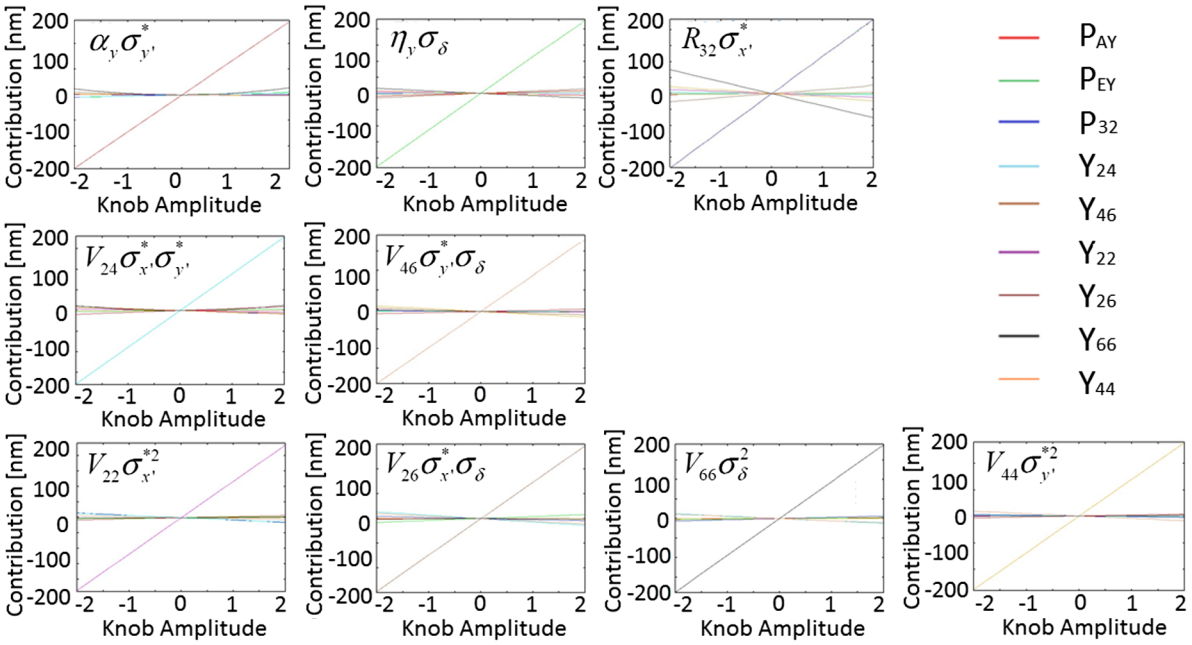

FIG. 10. Simulation result showing the orthogonality of the linear and second order knobs. The strength of each knob is normalized so that setting a knob amplitude of 1 contributes 100 nm of vertical beam size at the IP. The simulation was written using the 1×1 optics.

where $\langle\,\rangle$ denotes an average over the tracked particle positions at the IP. The second order terms are also evaluated using the particle distributions at the IP. We define relevant beam parameters as

$$V_{22} = \langle (y - \langle y\rangle)(x' - \langle x'\rangle)^2\rangle / \langle (x' - \langle x'\rangle)^2\rangle, \tag{32}$$

$$V_{26} = \langle (y - \langle y\rangle)(x' - \langle x'\rangle)(\delta - \langle\delta\rangle)\rangle / \sqrt{\langle (x' - \langle x'\rangle)^2(\delta - \langle\delta\rangle)^2\rangle}, \tag{33}$$

and so on. The simulated results for the 1×1 optics are shown in Fig. 10. Vertical beam size growth contribution corresponding to each component $\alpha_y\sigma^*_{y'}$, $\eta_y\sigma_\delta$, $R_{32}\sigma^*_{x'}$, $V_{24}\sigma^*_{x'}\sigma^*_{y'}$, $V_{46}\sigma^*_{y'}\sigma_\delta$, $V_{22}\sigma^{*2}_{x'}$, $V_{26}\sigma^*_{x'}\sigma_\delta$, $V_{66}\sigma^2_\delta$, and $V_{44}\sigma^{*2}_{y'}$ is shown as a function of the strengths of the tuning knobs. The strength of each knob is normalized to have 100 nm IP vertical beam size contribution $\Delta\sigma^*_y$ with a knob amplitude of 1. The vertical axis is the IP vertical beam size

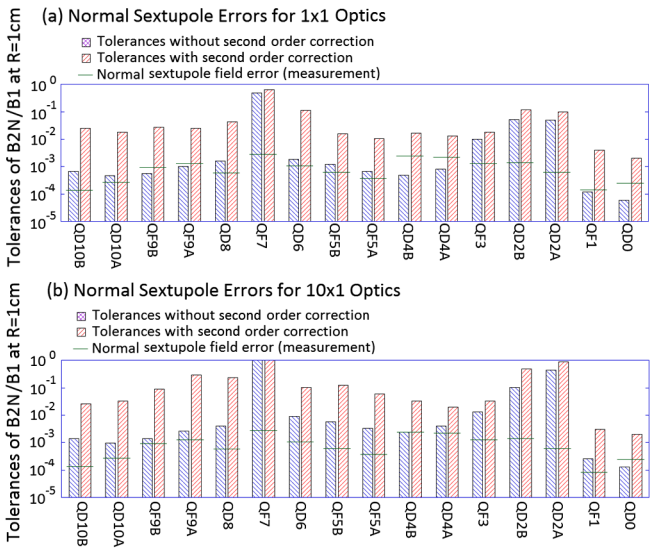

FIG. 11. Tolerances of normal sextupole field errors for quadrupole magnets in the 1×1 optics (a) and the 10×1 optics (b). The tolerances are defined by the requirement to induce a 2% IP vertical beam size growth, and the tolerances with and without second order knob corrections are shown. The measured normal sextupole field errors are also shown.

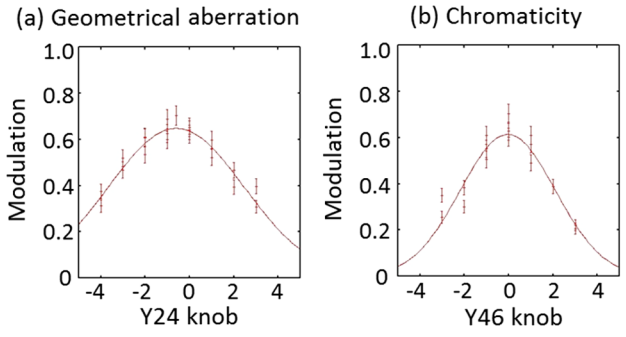

FIG. 12. Example use of nonlinear knobs utilizing strength changes of normal sextupole magnets in the final focus beam line. The beam size tuning was done with IP-BSM 30° mode.

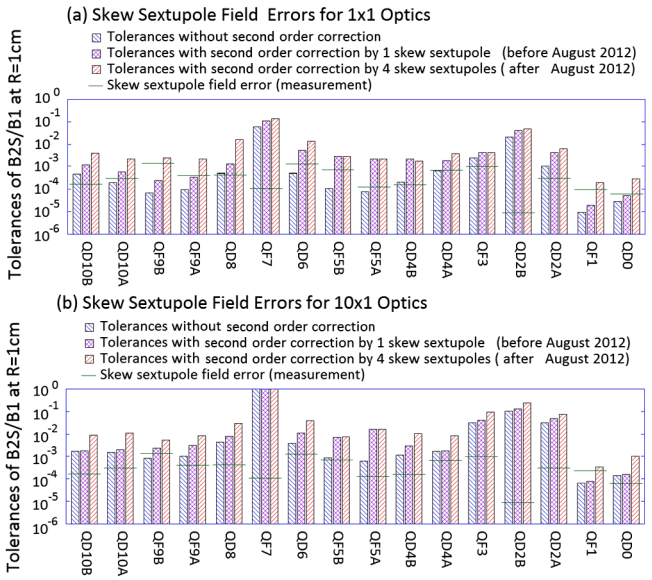

FIG. 13. Tolerance to skew sextupole field errors in ATF2 magnets for the (a) 1×1 optics and (b) 10×1 optics. The tolerances are defined by the requirement to induce a 2% beam size growth. Tolerances without second order knob correction, with correction by single skew sextupole, and with correction by four skew sextupoles are shown. Measured skew sextupole field errors are also shown.

contribution. This simulation demonstrates a satisfactory level of orthogonality for the first and second order knobs.

B. Beam size tuning with second order optics knobs

Figure 11 shows the tolerances of the normal sextupole field errors for the 1×1 optics and 10×1 optics with and without the second order optics knob tuning (Y_{24} and Y_{46} knobs). The second order optics knobs were applied twice in the tolerance calculations. The results of the magnetic field measurements are also shown in Fig. 11. The tolerances for the normal sextupole field errors are increased by using the second order knobs, and the measured sextupole field errors were within tolerance after

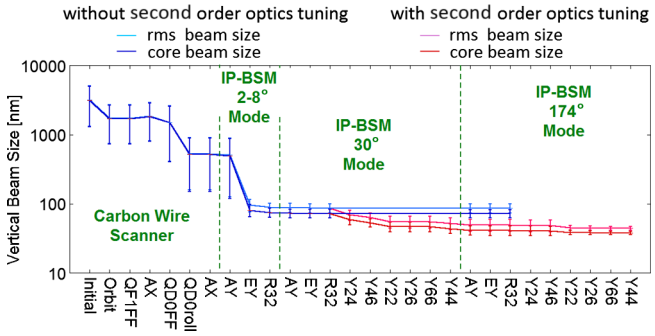

FIG. 14. The simulated results of beam size changes throughout the beam tuning process with and without second order optics knobs for the 1×1 optics. "rms beam size" is the standard deviation of the y distribution of the tracked particles at the IP. "Core beam size" is the width of a Gaussian function fitted to the core of this distribution.

the second order knob tuning both for the 1×1 optics and 10×1 optics. An example of the IP beam size tuning with the second order aberration knobs Y_{24} and Y_{46} is shown in Fig. 12.

Figure 13 shows the tolerances of the skew sextupole field errors for the 1×1 optics and 10×1 optics. The tolerances without second order knob correction, with correction by single skew sextupole and with correction by four skew sextupoles are shown in Fig. 13. The second order optics knobs were applied twice in the tolerance calculations. Results of the magnetic field measurements are also shown in Fig. 13. Tolerances of the skew sextupole field errors are increased by using the four skew sextupole magnets, especially for the final doublet (QF1 and QD0).

The beam tuning simulation including linear and second order knobs was carried out using SAD. The assumed error distributions in the simulation are shown in Table II. The simulation was performed using 100 random seeds. The initial beam tuning procedure in the simulation was assumed to be the same as the simulation with only the linear knobs (Fig. 7 and Table III). In the simulation, second order tuning was carried out using IP-BSM 30° and

TABLE IV. Simulated beam sizes with and without second order optics knobs for the original and present ATF2 optics. "rms beam size" is the standard deviation of the y distribution of the tracked particles at the IP. "Core beam size" is the width of a Gaussian function fitted to the core of this distribution. The $\pm$ shows the standard deviation of the simulated beam size at the IP.

				$\sigma_x^*[\mu\text{m}]$		$\sigma_y^*[\text{nm}]$	
	β_x^*	β_y^*		r.m.s.	core	r.m.s.	core
Original (1×1 optics)	4 mm	0.1 mm	Design	2.83 (linear optics)		34.6 (linear optics)	
			Linear	4.17 ± 0.32	3.50 ± 0.26	86.9 ± 13.2	72.2 ± 10.1
			Linear + 2nd order	4.07 ± 0.31	3.43 ± 0.22	44.3 ± 2.5	37.9 ± 1.8
Present (10×1 optics)	40 mm	0.1 mm	Design	8.94 (linear optics)		34.6 (linear optics)	
			Linear	9.24 ± 0.07	9.16 ± 0.07	47.1 ± 2.5	43.5 ± 1.6
			Linear + 2nd order	9.24 ± 0.07	9.16 ± 0.06	36.5 ± 0.9	36.0 ± 0.9

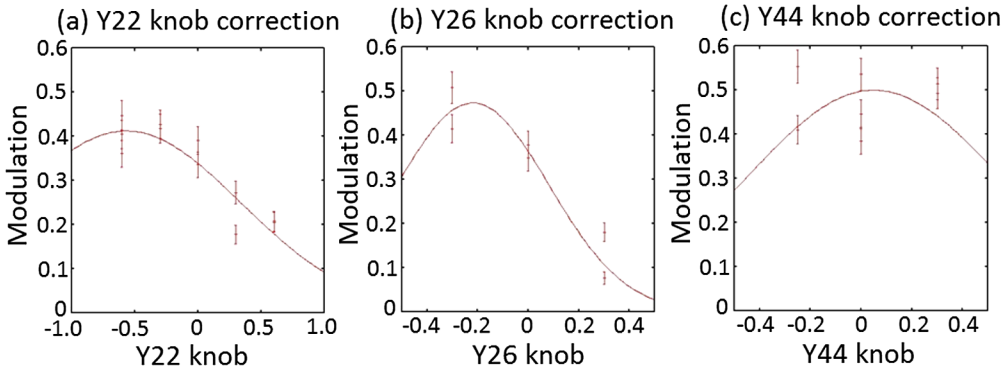

FIG. 15. Second order optics knob corrections with skew sextupole magnets in December 2012. Corrections were made to maximize the IP-BSM modulation depth in 30° mode.

174° modes after application of the linear knob tuning procedure. Beam size changes throughout the tuning for the 1×1 optics are shown in Fig. 14. The final beam sizes achieved for the 1×1 and 10×1 optics are shown in Table IV. Both the rms and core IP vertical beam size can be tuned below 40 nm for the 10×1 optics by including the use of the second order optics knobs. Furthermore, the core IP vertical beam size for the 1×1 optics is expected to also be reduced below 40 nm in this case. The rms beam size for the 1×1 optics is larger than the core beam size because of the beam tail generated by the higher order multipole fields of QF1 (see Fig. 3), but the rms beam size is also expected to be less than 50 nm. Since the rms beam size is sensitive to the beam tail, the rms beam size is larger than the core beam size. On the other hands, the IP-BSM is most sensitive to the beam size around 50 nm for 174° mode [$M = 0.5$ in Eq. (2)]. Therefore, when the beam size is less than 50 nm, the evaluated beam size by IP-BSM is in between the core beam size and the rms beam size.

C. Experimental results from beam size tuning

First observations of IP-BSM modulation in 174° mode were made in December 2012 with the 10×1 optics [13]. Since the dynamic range of IP-BSM 174° mode is less than 90 nm, the corresponding IP beam size was necessarily focused to less than 90 nm. The second order optics knobs were implemented during December 2012 operations. IP beam size optimization using the second order optics knobs Y_{22}, Y_{26}, and Y_{44} are shown in Fig. 15. Since the IP beam size contribution from the Y_{66} knob is not expected to be significant and the dynamic range is small, only Y_{22}, Y_{26}, and Y_{44} knobs were scanned.

Figure 16 shows the required strengths of the skew sextupole corrector magnets to correct for the case where each quadrupole magnet has a skew sextupole field $K_{2S} = 1\ \mathrm{m}^{-2}$ (with the 10×1 optics). The source of skew sextupole field error can be investigated by analyzing the settings of the skew sextupole correctors, SK1-SK4, after beam size tuning. Since the strengths of the skew sextupole magnets after the beam size tuning were much larger than that expected from magnetic measurements, we searched for an error source by analyzing the strength of the skew sextupole magnets during the December 2012 operation period. Since one of the candidates for the field error source was the strongest sextupole magnet (SD4), the impedances of all coils of the magnet were measured. It was, then, found that 1 coil of the magnet was shorted. Therefore, the shorted sextupole magnet was swapped with the weakest sextupole magnet (SF5). After the magnet swapping, the IP beam size was improved, and IP-BSM modulation in 174° mode has been observed without skew sextupole corrections. Figure 17 shows the results of second order optics corrections with skew sextupole magnets after the swapping. The optimum settings of the second order optics knobs Y_{22}, Y_{26}, and Y_{44} were

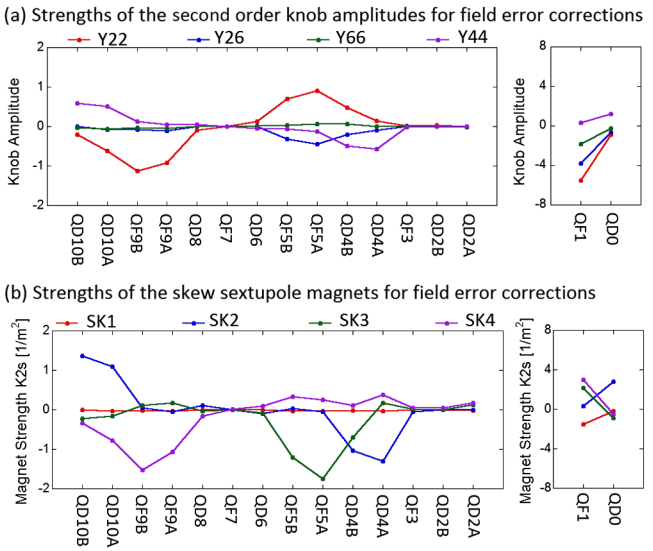

FIG. 16. Required strengths of the skew sextupole magnets to compensate for the case where each quadrupole magnet has a skew sextupole field $K_{2S} = 1\ \mathrm{m}^{-2}$, in the 10×1 optics. (a) Strength of the tuning knobs and (b) strength of each correction magnet.

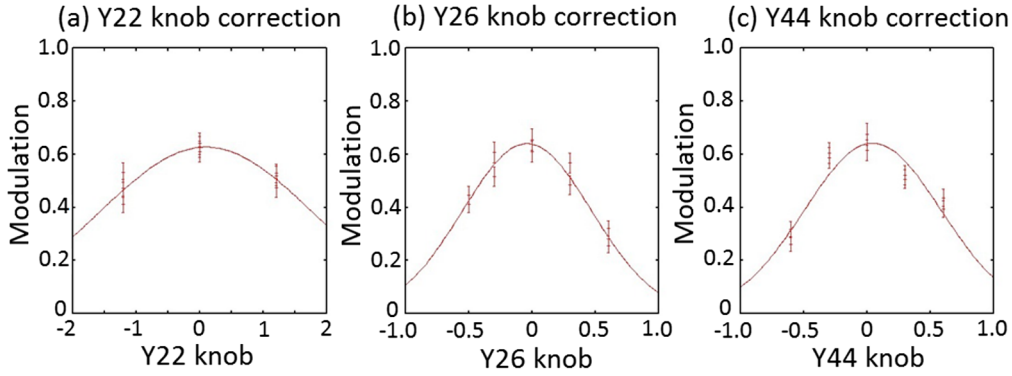

FIG. 17. Second order optics knob corrections with skew sextupole magnets in March 2013 (after magnet swapping). Corrections were made to maximize IP-BSM modulation in 30° mode.

approximately zero. This indicates that the skew sextupole field error in the ATF2 final focus beam line was reduced after the magnet swapping.

The maximum modulation depth, using IP-BSM 30° mode, was measured in March 2013, and was maintained throughout two consecutive weeks of operation. The maximum IP-BSM modulation depths with 174° mode were almost 30% [13]. The evaluated vertical beam size at the IP, assuming $C = 1$ in Eq. (2) is about 65 nm and represents an upper limit of the focused beam size.

V. SUMMARY

The final focus scheme of ILC is being tested using the ATF2 beam line. To achieve nm-scale beam sizes, we are using tuning knobs that change both the linear and second order optics. The linear optics tuning knobs use orthogonal sets of horizontal and vertical position changes of sextupole magnets. The second order optics knobs use almost orthogonal sets of strength changes of sextupole magnets and skew sextupole magnets, which were installed to correct skew sextupole field errors. By using these optics tuning knobs, the tolerances of skew sextupole field errors were increased and a vertical beam size at the IP of below 50 nm, even for the original ATF2 optics (1×1 optics), is expected with field errors given by the magnetic field measurements. Furthermore, the skew sextupole settings allowed us to locate a source of skew sextupole field errors. We succeeded to observe modulations with IP-BSM 174° mode in December 2012 with the present ATF2 optics (10×1 optics) by using second order optics corrections with the skew sextupole magnets. After we removed the field error source, the skew sextupole field error in the ATF2 beam line became insignificant and the IP vertical beam size could be focused to less than 65 nm.

ACKNOWLEDGMENTS

We would like to thank to all of the group members of the ATF Collaboration, especially for the ATF2 beam tuning group, R. Ainsworth, T. Akagi, J. Alabau, A. Aryshev, S. Bai, O. Blanco, N. Blaskovic, S. Boogert, L. Corner, M. Davis, A. Jeremie, Y. I. Kim, S. Liu, A. Lyapin, D. McCormick, H. G. Morales, J. Nelson, Y. Renier, J. Pfingstner, J. Resta-Lopez, J. Snuverink, R. Tanaka, and J. Yan. Furthermore. We also thank C. Spencer for magnetic field measurement of ATF2 magnets, D. Wang for the modeling of the multipole field errors, and K. Oide, S. Yamaguchi, and A. Yamamoto for their invaluable support of the ATF2 project.

[1] ATF2 Group, KEK-Report No. 2005–2, 2005.
[2] P. Bambade *et al.*, Phys. Rev. ST Accel. Beams **13**, 042801 (2010).
[3] ILC Global Design Effort, ILC Technical Design Report, 2013, http://www.linearcollider.org/ILC/Publications/Technical-Design-Report.
[4] K. Kubo *et al.*, Phys. Rev. Lett. **88**, 194801 (2002).
[5] Y. Honda *et al.*, Phys. Rev. Lett. **92**, 054802 (2004).
[6] P. Raimondi and A. Seryi, Phys. Rev. Lett. **86**, 3779 (2001).
[7] T. Shintake, Nucl. Instrum. Methods Phys. Res., Sect. A **311**, 453 (1992).
[8] V. Balakin *et al.*, Phys. Rev. Lett. **74**, 2479 (1995).
[9] T. Suehara *et al.*, Nucl. Instrum. Methods Phys. Res., Sect. A **616**, 1 (2010).
[10] A. Seryi, M. Woodley, and P. Raimondi, Report No. SLAC-PUB-9895.
[11] SAD is a computer program for accelerator design; see http://acc-physics.kek.jp/SAD/.
[12] E. Marin *et al.*, Report No. CERN-ATS-2011-122.
[13] G. White *et al.*, Phys. Rev. Lett. **112**, 034802 (2014).